Frequency domain 3-D electromagnetic migration and imaging of sea-bottom geoelectrical structures

Le Wan, Pechet Puahengsup, and Michael S. Zhdanov, Department of Geology and Geophysics, University of Utah*

Summary

In this paper we develop a fast 3-D electromagnetic (EM) migration method for marine geophysical exploration. The developed migration algorithm is based on downward extrapolation of the observed EM field using a special form of finite-difference equation for the migration field. It allows us to migrate within the sea-bottom formations the EM signals observed by the sea-bottom receivers. The migration field is subsequently transformed in the resistivity image of the sea-bottom geoelectrical structures. This technique is in an order faster than the conventional inversion. It can be used for fast imaging of the marine magnetotelluric (MT) and controlled-source electromagnetic (CSEM) data in off-shore hydrocarbon (HC) exploration.

Introduction

There is growing interest in developing fast interpretation methods for marine controlled-source electromagnetic (MCSEM) data. Over the last few years several papers have been published dedicated to imaging MCSEM data using EM migration (e.g., Tompkins, 2004; Mittet et al., 2005; Wan and Zhdanov, 2005a, b; Zhdanov et al., 2006).

In this paper we present new results of developing a fast 3-D EM migration method for marine geophysical exploration. We extend the method and numerical algorithm of frequency domain (FD) 2-D EM migration, developed by Wan and Zhdanov (2005a, b) for full 3-D migration. We present several numerical examples of the practical application of this technique for fast imaging of a sea-bottom hydrocarbon (HC) reservoir.

EM migration in frequency domain

Consider a 3-D geoelectrical model with a background electrical conductivity $\sigma = \sigma_b$ and a local inhomogeneity D with a conductivity $\sigma = \sigma_b + \Delta\sigma$, varying spatially. The background conductivity is formed by a horizontally layered model consisting of nonconductive air, a conductive sea-water layer, and the homogeneous part of a sea-bottom formation.

The electric field in this model can be represented as a superposition of two fields: the primary field $\mathbf{E}^d$, that propagates downward into the sea bottom, and the secondary field, $\mathbf{E}^u$, which is scattered upward from the sea-bottom inhomogeneities:

$$\mathbf{E} = \mathbf{E}^d + \mathbf{E}^u, \tag{1}$$

where the downward- and upward-going fields can be expressed approximately as follows (Zhdanov et al., 1996):

$$\mathbf{E}^d = \mathbf{Q}^d(x,y,z)\, e^{ik_b z}, \text{ and } \mathbf{E}^u = \mathbf{Q}^u(x,y,z)\, e^{-ik_b z}, \tag{2}$$

and k_b is the wave number for the sea-bottom layer ($\mathrm{Re}\, k_b \geq 0$). Substituting (2) into (1), we obtain:

$$\mathbf{E}(x,y,z) \approx \mathbf{Q}^d(x,y,z)\, e^{ik_b z} + \mathbf{Q}^u(x,y,z)\, e^{-ik_b z},\ 0 \leq z \leq h_D, \tag{3}$$

We can see from equations (2) and (3) that the amplitude of downward-going field $\mathbf{E}^d$ decays with the depth, while the amplitude of the up-going field $\mathbf{E}^u$ increases with the depth. It is possible to separate the electric field measurements at the sea bottom into up-going and down-going fields (Berdichevsky and Zhdanov, 1984; Zhdanov, 1988). We can transform the up-going part of the electric field for imaging seabed structures by downward extrapolating this field inside the sea bottom. This transformation, however, is very unstable due to the exponential increase of noise in the data with the depth of the downward continuation. Zhdanov et al. (1996) have suggested, instead, to downward propagate the up-going part of the field using the original diffusion equation. Mathematically this means that we introduce a new EM field, called *electromagnetic migration field* $\mathbf{E}^m$,which satisfies the following equation:

$$\nabla\times(\nabla\times\mathbf{E}^m) - k_b^2\mathbf{E}^m = 0,\ z \geq 0, \tag{4}$$

and the boundary condition at the sea bottom:

$$\mathbf{E}^m|_{z=0} = \mathbf{E}^u|_{z=0} = \mathbf{Q}^u(x,y,0)\,. \tag{5}$$

In other words, the EM migration field $\mathbf{E}^m$ is a solution of the boundary value problem for equation (4) within the entire low half-space. It can be shown that this solution has the form:

$$\mathbf{E}^{m*}(x,y,z,\omega) = \mathbf{Q}^m(x,y,z,\omega)e^{-k_b z},\ 0 < z < +\infty \tag{6}$$

where asterisk "*" denotes a complex conjugate value.

Finite difference migration of 3-D EM field

Zhdanov et al., (1996) have developed an efficient algorithm for the finite-difference migration of the 2-D EM field. In this paper we extend this method for 3-D case. According to equation (6), one can find the migration field

if the function $\mathbf{Q}^m(x,y,z,\omega)$ is known. This function can be calculated at different levels inside the sea bottom using a 3-D finite-difference technique similar to one developed by Zhdanov et al. (1996) for 2-D fields.. It can be demonstrated that the corresponding scalar components Q of function $\mathbf{Q}^m$ satisfy the equation:

$$\frac{1}{2k_b}\left(\frac{\partial^2}{\partial x^2}+\frac{\partial^2}{\partial y^2}\right)\frac{\partial Q}{\partial z}+\left(\frac{\partial^2}{\partial x^2}+\frac{\partial^2}{\partial y^2}\right)Q-2k_b\frac{\partial Q}{\partial z}=0. \tag{7}$$

Let us introduce a discrete function $Q(i,l,j) = Q(x_i,y_l,z_j,\omega)$ on the rectangular grid $\Sigma(x_i,y_l,z_j)$, $i = 1,2,...N_x$, $l = 1,2,...N_y$, $j = 1,2,...N_z$, and a discrete function $k_{ilj} = k_n(x_i,y_l,z_{j+1/2})$, on the auxiliary grid $\widetilde{\Sigma}(x_i,y_l,z_{j+1/2})$ where $z_{j+1/2} = z_j + \Delta z_j/2$. We then rewrite equation (7) as an approximate finite-difference equation on the auxiliary grid $\widetilde{\Sigma}$. Representing the derivatives of Q approximately in terms of the discrete functions $Q(i,l,j)$ and k_{ilj}, we obtain the following finite-difference equation for $Q(i,l,j)$:

$$a_{ilj}Q(i+1,l,j+1)+a_{ilj}\left(\frac{\Delta x_i}{\Delta y_l}\right)^2 Q\,(i,l+1,j+1)$$

$$+A_{ilj}Q(i,l,j+1)+a_{ilj}\frac{\Delta x_i}{\Delta x_{i-1}}Q\,(i-1,l,j+1)$$

$$+a_{ilj}\left(\frac{\Delta x_i}{\Delta y_l}\right)^2\frac{\Delta y_l}{\Delta y_{l-1}}Q\,(i,l-1,j+1)=D_{ilj}, \tag{8}$$

where $i = 2,3,...N_x-1$, $l = 2,3,...N_y-1$, $j = 1,2,...N_z-1$,

$$D_{ilj}=b_{ilj}Q(i+1,l,j)+b_{ilj}\left(\frac{\Delta x_i}{\Delta y_l}\right)^2 Q\,(i,l+1,j)$$

$$+B_{ilj}Q(i,l,j)+b_{ilj}\frac{\Delta x_i}{\Delta x_{i-1}}Q\,(i-1,l,j)$$

$$+b_{ilj}\left(\frac{\Delta x_i}{\Delta y_l}\right)^2\frac{\Delta y_l}{\Delta y_{l-1}}Q\,(i,l-1,j) \tag{9}$$

and coefficients a_{ilj}, b_{ilj}, A_{ilj}, B_{ilj} are equal to:

$$a_{ilj}=\frac{1}{2}\left[\frac{1}{\Delta z_j k_{ilj}}+1\right],\ b_{ilj}=\frac{1}{2}\left[\frac{1}{\Delta z_j k_{ilj}}-1\right].$$

$$A_{ilj} = -a_{ilj}\left(1+\frac{(\Delta x_i)^2}{\Delta x_i\Delta x_{i-1}}+\frac{(\Delta x_i)^2}{(\Delta y_l)^2}+\frac{(\Delta x_i)^2}{\Delta y_l\Delta y_{l-1}}\right) -\frac{2k_{ilj}(\Delta x_i)^2}{\Delta z_j}$$

$$B_{ilj} = -b_{ilj}\left(1+\frac{(\Delta x_i)^2}{\Delta x_i\Delta x_{i-1}}+\frac{(\Delta x_i)^2}{(\Delta y_l)^2}+\frac{(\Delta x_i)^2}{\Delta y_l\Delta y_{l-1}}\right) -\frac{2k_{ilj}(\Delta x_i)^2}{\Delta z_j}.$$

Note that, if the discrete function $Q(i,l.j)$ is known at a level j, one can find the coefficients D_{ilj} from equation (9). Therefore, equation (8) becomes a system of linear equations with respect to the values $Q(i,l,j+1)$ of the discrete function at the next level, $j+1$. We also have the boundary condition (5) at the observation surface:

$$\mathbf{Q}^m(i,l,1)=\mathbf{E}^u\,(x_i,y_l,0)\,,\ i=1,2,..N_x,$$

and boundary conditions for the values of the function $Q(i,l,j)$ at the left and right and back and front boundaries of the area of migration. The boundary values on the left, right, back and front sides of the migration domain can be obtained by a simple 1-D migration of the electric field downward at the sides of the observation area using simple formulae:

$$\begin{aligned}\mathbf{E}^{m*}(x,y_B,z) &= \mathbf{E}^u\,(x,y_B,0)\,e^{-k_b z},\\ \mathbf{E}^{m*}(x,y_F,z) &= \mathbf{E}^u\,(x,y_F,0)\,e^{-k_b z},\\ \mathbf{E}^{m*}(x_L,y,z) &= \mathbf{E}^u\,(x_L,y,0)\,e^{-k_b z},\end{aligned}$$

$$\mathbf{E}^{m*}(x_R,y,z)=\mathbf{E}^u\,(x_R,y,0)\,e^{-k_b z},\ 0<z<+\infty. \tag{10}$$

After all the values $Q(i,l,j)$ are found, we compute the migration field $\mathbf{E}^m$ in the nodes of grid $\Sigma(x_i,y_l,z_j)$, using equation (6):

$$\mathbf{E}^m(x_i,y_l,z_j)=\mathbf{Q}^m(i,l,j)e^{-k_b z_j},\quad i=1,2,...N_x,\ l=1,2,...N_y,\ j=1,2,...N_z. \tag{11}$$

Examples of EM migration and imaging of marine EM data

We will present below the results of numerical application of the developed algorithm to synthetic and field marine MT and CSEM data.

A simplified geoelectrical model of the TWGP survey area

We consider first a synthetic model simulating the MCSEM survey in the Troll West Gas Province (TWGP), Offshore Norway (Amundsen et al., 2004). The survey consists of 24 receivers, deployed along a line crossing the Oil Province, the Western Gas Province, and the Eastern Gas Province of the Troll Field.

First we consider a simplified geoelectrical model of the TWGP survey area. The gas reservoir is approximated by a 7,000 m x 10,000 m x 100 m prismatic body with a resistivity of 250 Ohm-m. It is located below the sea bottom at a depth of 1,100 m within conductive sediments with a resistivity of 1 Ohm-m. The sea layer has a 300 m depth with a resistivity of 0.2 Ohm-m. Forty-one receivers are located at the sea bottom at 500 m intervals along a 20,000 m profile. The 230-m-long bipole electric transmitter is moving 40 m above the sea bottom in the x direction, transmitting a signal every 500 m. The operating frequencies are 1.75, 1.25, 0.75, and 0.25 Hz. We use the INTEM3D code for computing the E_x component of the electric field in the receivers. Figure 1 shows a side view of the model described above.

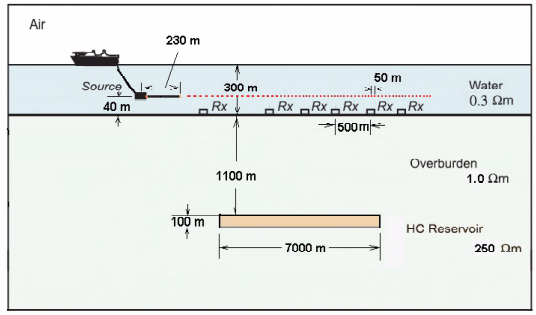

Fig. 1: A simplified geoelectrical model of the TWGP survey area.

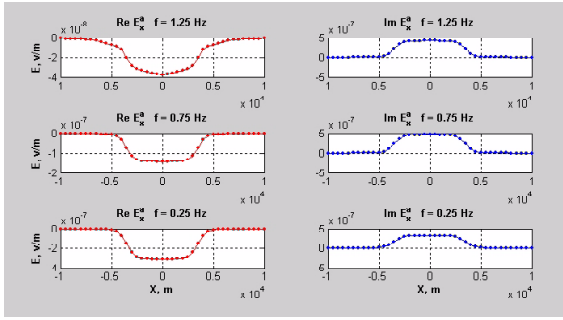

Fig. 2: The plots of the stacked anomalous electric fields E_x for different frequencies.

Now we have stacked the anomalous parts of the electric field data observed in the receivers and the normal (background) parts separately. The plots of the stacked anomalous electric fields for different frequencies are shown in Figure 2.

The stacked anomalous electric fields were migrated in the lower half-space using a simplified 2-D version of the finite-difference migration algorithm introduced above. The corresponding migration resistivity of the seabed, ρ_{sb}, was calculated using the imaging conditions introduced by Zhdanov et al., 1996.

Figure 3 presents the final migration image of the simplified geoelectrical model of the TWGP reservoir obtained by 2-D migration of the synthetic MCSEM data. One can see a good reconstruction of the reservoir in the migration image.

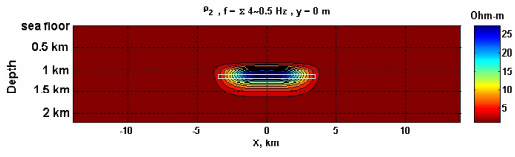

Fig. 3: A resistivity image of the simplified geoelectrical model of the TWGP reservoir obtained by 2-D migration of the synthetic MCSEM data.

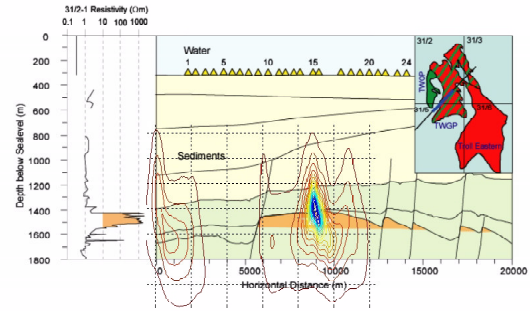

Fig. 4: A simplified geological model along the survey line in the Troll West Gas Province (TWGP), offshore Norway, overlaying the resistive structure obtained by the 2-D migration.

2-D migration of the practical TWGP MCSEM data

The practical TWGP data were collected using 24 sea-bottom receivers. For every receiver, we used the data with the maximum transmitter-receiver offset of 5 km. We also used the field data for one frequency of 0.25 Hz. According to the reciprocity principle, the electric field data observed in the receiver for a given transmitter are equal to the electric field produced by a reciprocal transmitter located in the true receiver position and measured in the true transmitter location. We have applied this reciprocity principle to every receiver. The anomalous parts of the reciprocal fields are migrated downward using the 2D finite-difference migration code. We have also calculated the average background field in the reciprocal receivers, which is required for the migration imaging. The migration reciprocal fields for all receivers are stacked together. This stacked field was used for the final resistivity imaging. Figure 4 shows a simplified geological model along the survey line in the Troll West Gas Province (TWGP), offshore Norway, overlaying the resistive structure obtained by the 2-D migration.

The image is not as good as for the synthetic model. However, the location of the gas reservoir is clearly identified in this figure. Note that we have used just one frequency for the practical data migration. The previous theoretical and model studies clearly indicate that the multi-frequency migration produces a much better result than a single frequency migration. In future, we plan to apply the migration method to multi-frequency field data as well.

3-D migration of the array marine EM data for reconnaissance surveys

In this section we investigate the full 3-D finite-difference migration. For the sake of simplicity, we apply this algorithm to the synthetic marine MT data only. Future research will be focused on numerical study of the MC-

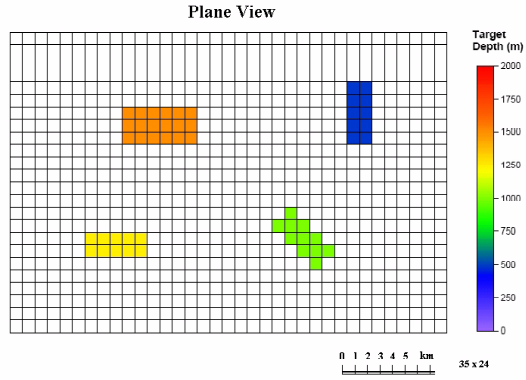

Fig. 5: A plane view of a geoelectrical model used for testing the migration imaging of the EM data collected by the reconnaissance marine MT survey.

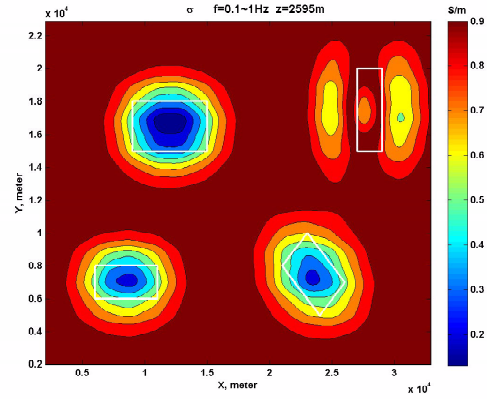

Fig. 6: A horizontal slice of the 3-D migration resistivity image at $z = 2595$ m.

SEM data.

There is a possibility of using the marine MT and CSEM data as reconnaissance surveys in HC exploration. The migration imaging can be an appropriate tool for fast imaging of the results of these surveys. As an example, we consider a more complicated geoelectrical model, containing four different reservoirs with the different sizes and at different depths (see Figures 5).

The first reservoir is represented by a rectangular 6000 m x 3000 m x 100 m body with the top surface of the reservoir at a depth of 1500 m below the sea bottom. Reservoir # 2 has a size of 2000 m x 5000 m x 100 m, and it is located at a depth of 500 m below the sea bottom. Reservoir #3 with a size of 5000 m x 2000 m x 100 m located at 1000 m below the sea bottom. The fourth reservoir, with a size of 2000 m x 4000 m x 100 m, is at a depth of 800 m below sea bottom. The seawater depth is 1500 m. It has a resistivity of 0.3 Ohm-m, the resistivity of the sea-bottom sediments is 1 Ohm-m, and all four reservoirs have the same resistivity: 100 Ohm-m.

There are 204 receivers (17 x 12) at the sea bottom separated by 2000 m in both the x and y directions. The electric components of the MT field (the telluric electric field) in the receivers were computed with the INTEM3D forward modeling code for 9 frequencies: 0.1, 0.25, 0.5, 0.75, 1.0, 2.5, 5.0, 7.5, and 10 Hz.

We use the same 3-D finite-difference (FD) migration algorithm discussed in the previous sections to generate a 3-D migration resistivity image. Figure 6 shows the horizontal slice of this volume image at $z = 2595$ m. We can clearly see all four reservoirs in this image.

Conclusions

We have developed a fast 3-D finite-difference migration imaging algorithm. This method is based on the extension for a 3-D case of the 2-D one-way downward extrapolation technique developed by CEMI in the past. It allows us to migrate within the sea-bottom formations the EM signals observed by the sea-bottom receivers. The migration field is subsequently transformed in the resistivity image of the sea-bottom geoelectrical structures.

We have demonstrated that this method can be used for fast imaging of marine MT and CSEM data. In the case of an array EM observation, migration can be used as a reconnaissance tool in off-shore HC exploration.

Acknowledgments

The authors acknowledge the support of the University of Utah Consortium for Electromagnetic Modeling and Inversion (CEMI), which includes BAE Systems, Baker Atlas Logging Services, BGP China National Petroleum Corporation, BHP Billiton World Exploration Inc., British Petroleum, Centre for Integrated Petroleum Research, EMGS, ENI S.p.A., ExxonMobil Upstream Research Company, INCO Exploration, Information Systems Laboratories, MTEM, Newmont Mining Co., Norsk Hydro, OHM, Petrobras, Rio Tinto - Kennecott, Rocksource, Russian Research Center Kurchatov Institute, Schlumberger, Shell International Exploration and Production Inc., Statoil, Sumitomo Metal Mining Co., and Zonge Engineering and Research Organization.

We are thankful to the Troll license group consisting of Statoil, Norsk-Hydro, Petoro, Norske Shell, Total, and ConocoPhillips, for providing the TWGP SBL data and for permission to publish the result.